

The beads-on-string structure of viscoelastic threads

By **Christian Clasen**^{1,5}, **Jens Eggers**^{2,6}, **Marco A. Fontelos**³, **Jie Li**⁴,
and **Gareth H. McKinley**¹

¹Hatsopoulos Microfluids Lab, Department of Mechanical Engineering, MIT, Cambridge,
Mass. 02139, USA

²Universität Gesamthochschule Essen, Fachbereich Physik, 45117 Essen, Germany

³Departamento de Ciencia e Ingenieria, Universidad Rey Juan Carlos, C/ Tulipán S/N, 28933
Móstoles, Madrid, Spain.

⁴BP Institute & Engineering Department, University of Cambridge, Madingley Road
Cambridge, CB3 0EZ, United Kingdom

⁵present address: Institut für Technische und Makromolekulare Chemie, Bundesstr. 45, 20146
Hamburg, Germany

⁶present address: School of Mathematics, University of Bristol, University Walk,
Bristol BS8 1TW, United Kingdom

(Received 2003 and in revised form August 2, 2005)

By adding minute concentrations of a high molecular weight polymer, liquid jets or bridges collapsing under the action of surface tension develop a characteristic shape of uniform threads connecting spherical fluid drops. In this paper, high-precision measurements of this beads-on-string structure are combined with a theoretical analysis of the limiting case of large polymer relaxation times and high polymer extensibilities, for which the evolution can be divided into two distinct regimes. For times smaller than the polymer relaxation time, over which the beads-on-string structure develops, we give a simplified local description, which still contains the full complexity of the problem. At times much larger than the relaxation time, we show that the solution consists of exponentially thin-

ning threads connecting almost spherical drops. Both experiment and theoretical analysis of a one-dimensional model equation reveal a self-similar structure of the corner where a thread is attached to the neighbouring drops.

1. Introduction

Understanding the behaviour of polymeric free-surface flows is of enormous importance for a wide variety of applications in the chemical processing, food and consumer products industries. Operations such as ink jet printing, spraying of fertilisers, paint-levelling, misting, bottle-filling and roll coating are all controlled by interactions between the non-Newtonian stresses in the bulk and capillary stresses at the deformable free-surface. Long-chained macromolecules are also ubiquitous in biological fluids, and very significantly affect the corresponding free-surface dynamics. If one places a small drop of saliva between two fingers and pulls them apart, the resulting liquid bridge does not collapse, but an extremely fine thread remains for several seconds. The lifetime of this bridge is intimately connected with the molecular weight and conformation of the proteins (mucins) and hormones in the saliva. Measurement of filament lifetimes in biofluids such as mucus or saliva can be used as a fertility indicator (Kopito & Kosasky (1979)).

A number of recent studies have promulgated the idea of using the capillarity-induced thinning of a liquid filament as a rheometric device for quantifying the properties of complex fluids in predominantly extensional flows (Bazilevsky et al. (1990), Stelter et al. (2000), Tripathi et al. (2000)). A typical configuration is shown in figure 1. A cylindrical liquid bridge of the fluid to be tested is initially formed between two coaxial cylindrical plates. In the present experiment, the test fluid is an ideal elastic fluid consisting of a dilute solution of monodisperse high molecular weight polystyrene dissolved in a viscous

solvent. Details of the rheological characterisation of the test fluid are provided in Appendix A. A step uniaxial strain is imposed on the bridge to extend it beyond the static (Plateau) stability limit. The liquid filament subsequently undergoes a capillary-thinning process toward a final breakup event. The no-slip boundary condition at the endplates retards the radial flow near the end plates and thus imposes a well-defined initial axial perturbation or ‘neck’ on the liquid column which controls the location of the subsequent necking process. The time evolution in the local filament radius is monitored optically using either a laser micrometer or high-speed video-imaging.

To convert such measurements of filament evolution into an extensional viscosity it is necessary to understand the balance of forces acting on the fluid filament. The slenderness of the fluid thread induced by the step strain means that a one-dimensional approximation to the equations can be useful in the analysis. Entov & Hinch (1997) provide a detailed discussion of the evolution of a perfectly cylindrical thread of viscoelastic fluid undergoing capillary-driven thinning and breakup. Their analysis shows that there can be a lengthy intermediate regime in which inertial, viscous and gravitational forces are all negligible and elastic and capillary forces balance each. Capillary pressure drives the thinning process whilst fluid viscoelasticity resists the necking of the fluid thread. To prevent the molecules from relaxing the radius must continuously decrease in time at a rate that is directly related to the characteristic relaxation rate of the polymer solution. In this regime the local extension rate in the neck is constant and the radius of the filament decreases exponentially in time. Measurement of this rate of thinning thus enables a direct determination of the characteristic relaxation time of the viscoelastic fluid. Such observations have been found to be in quantitative agreement with data obtained in extensional rheometers (Anna & McKinley (2001)). The extensional flow in the thread also results in a net tensile force in the filament which has, to date, been neglected. In the

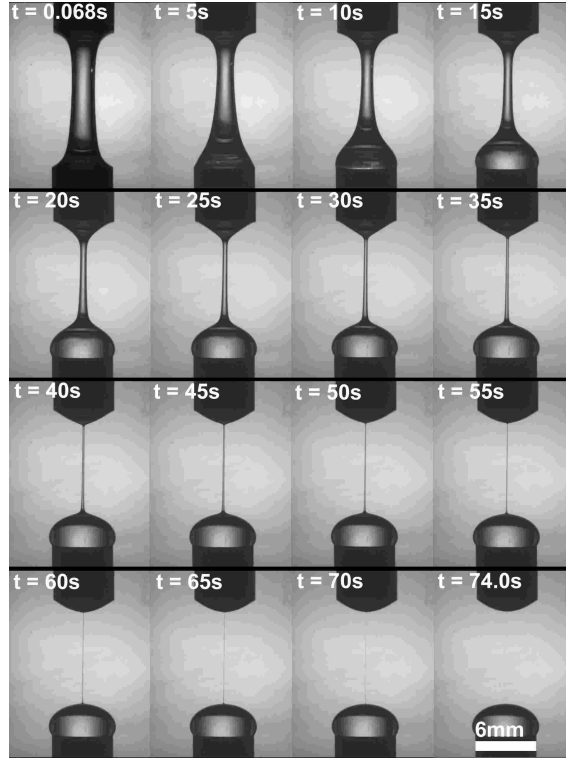


FIGURE 1. Experimental images of a collapsing liquid bridge of polymer solution in a viscous solvent (plate radius $R_0 = 3 \text{ mm}$, distance 13.8 mm). This state was obtained by rapidly stretching the liquid bridge from an initial gap of 3 mm width, which was completely filled with fluid. The surface tension is $\gamma = 37 \text{ mN/m}$, the density $\rho = 1026 \text{ kg/m}^3$. The solvent and polymeric contributions to the viscosity are $\eta_s = 65.2 \text{ Pas}$ and $\eta_p = 9.8 \text{ Pas}$, respectively, the polymer timescale is $\lambda = 8.1 \text{ s}$. Relative to the capillary timescale $\tau = \sqrt{\rho R_0^3 / \gamma}$ this results in a Deborah number of $De = 296$.

present work we determine this elastic tension in a self-consistent manner, by matching the cylindrical profile of the thinning thread to the hemispherical end caps. This reveals a new self-similar solution in the corner region formed by the thread and the end-caps, whose characteristic length scale is proportional to the thread radius.

A local elasto-capillary balance has also been observed in other experimental configurations including breakup of forced polymeric jets (Christanti & Walker (2002))

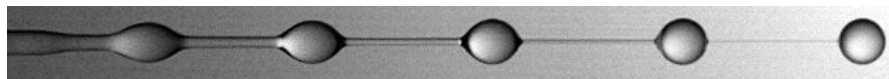


FIGURE 2. High speed video-image of a jet of dilute (0.01 *wt%*) aqueous polyacryamide solution (surface tension $\gamma = 62 \text{ mN/m}$) undergoing capillary thinning. The sharp-edged jet orifice is at the left of the image (radius $R_0 = 0.30 \text{ mm}$) and the free jet velocity is 30 cm/s . The polymeric contribution to the viscosity is $\eta_p = 0.0119 \text{ Pas}$, and the polymer timescale is found to be $\lambda = 0.012 \text{ s}$. This corresponds to a Deborah number of $De = 18.2$.

and gravity-driven drop formation in viscoelastic polymer solutions (Amarouchene et al. (2001), Cooper-White et al. (2002)). On close examination of a thinning viscoelastic jet, a string of tiny droplets can often be distinguished. This ‘beads on a string’ phenomenon was first described in Goldin et al. (1969), and has been reproduced in numerical simulations by Bousfield et al. (1986). A representative image of this viscoelastic jet break-up process is shown in figure 2. The jet consists of a series of cylindrical ligaments connecting spherical beads. As the jet is convected from left to right, fluid is forced by capillarity from the thinning ligaments into the spherical droplets. Most analytical studies of this structure have been performed using simplifying assumptions about the slenderness of the liquid jet, see Yarin (1993) for a review. However, despite a considerable number of studies (see e.g. Goren & Gottlieb (1982), Entov & Yarin (1984), Bousfield et al. (1986), Forest & Wang (1990), Shipman et al. (1991), Larson (1992), Renardy (1994), Renardy (1995), Chang et al. (1999)) a full analytical description of the beads-on-string phenomenon is still open, even in the context of one-dimensional models.

In this paper we seek a self-similar solution that encompasses the elasto-capillary balance documented in experimental observations in liquid bridges, pinching drops and thinning jets. We follow the spirit of some of the earlier work by employing two simplifying assumptions: first, we will consider the simplest canonical model for a dilute polymer

solution, the so-called Oldroyd-B model (e.g. Bird et al. (1987)), which can be derived from kinetic theory by treating a dilute solution of polymer chains as a suspension of non-interacting Hookean dumbbells. The simplifications resulting from such a description mean that the polymer solution exhibits a single relaxation time λ , and that the chains are infinitely stretchable. The one-dimensional analysis of Entov & Hinch (1997) considered the more general case of a relaxation modulus $G(t)$ comprising of a discrete spectrum of relaxation times (corresponding to a non-interacting suspension of dumbbells with different spring constants). As we note in Appendix A, incorporating their analysis with the Zimm relaxation spectrum measured for dilute solutions results in a rate of stretching in the liquid thread that is rapidly dominated by the dumbbells with the longest time constant. All of the other modes relax and do not contribute to the dominant balance, so the approximation of a single relaxation time is not considered to be too limiting. Furthermore, a number of recent experimental studies (e.g. Spiegelberg et al. (1996), Amarouchene et al. (2001), Anna & McKinley (2001)) have utilised model dilute polymer solutions which are indeed very well described by a single time scale over a wide range of extensions.

The additional assumption of infinite extensibility is bound to break down, even for very long polymers, as the ends of the chain diverge exponentially in an extensional flow. In fact, it has been shown by Renardy (1994) for the model to be treated in this paper (and neglecting inertia) that a thread can *never* break up in finite time. Entov & Hinch (1997) consider the Finitely Extensible Nonlinear Elastic Dumbbell (or FENE) model and show that for highly extensible molecules (as characterised by large values of the FENE extensibility parameter $b > 10^3$) there is a long intermediate elastic regime (which may extend for times of $10 - 20 \lambda$) in which neither the initial response of the solvent nor the finite length of the molecules is important and the chains indeed extend

effectively as infinitely extensible dumbbells with a single characteristic relaxation time. This has also been verified experimentally using a homologous series of polystyrene test fluids with solutes of increasing molecular weight (Anna & McKinley (2001)). In the present study, we therefore do not consider the final stages of breakup where the finite length of the polymers begins to affect the necking process. This final asymptotic regime has been considered for the FENE model by Entov & Hinch (1997), and more recently for the Giesekus model by Fontelos & Li (2004). In each case the extensional viscosity of the fluid is bounded and the filament radius ultimately decreases linearly in time. The initial onset of this regime can also be observed in the very last stages of the experimental measurements when the thread radius has reduced to $O(1 - 10 \mu m)$; however we do not include this data in our comparison between theory and experimental observation.

The second simplifying assumption is that we are treating the flow inside the fluid thread as effectively one-dimensional (e.g. Forest & Wang (1990)). This is consistent as long as the shape of the liquid column remains slender, i.e. the characteristic radial variations are small compared to the variation in the axial direction. This assumption is problematic near the ends of the fluid drops in the beads-on-string structure. Following Eggers & Dupont (1994), we hope to at least partially deal with this problem by keeping the *full* expression for the mean curvature in the Laplace pressure, which drives the breakup. This makes spherical drops exact static solutions of the equations, and ensures that at least the surface tension terms are correctly accounted for.

We are left with a model that treats the liquid column as a set of one-dimensional continuum equations for the fluid flow coupled with equations describing the state of stress of the polymer chains in solution. A typical experimental situation would be that of a jet ejected from a nozzle, or a liquid bridge held between two circular end-plates. In all of the following, we will choose the initial bridge or jet radius R_0 as a unit of length,

and the corresponding capillary time $\tau = (\rho R_0^3/\gamma)^{1/2}$ as the unit of time, where γ is the surface tension and ρ the density of the fluid. If $R_0 \approx 1\text{mm}$, τ is about 4 ms for a water-based solvent. Note that for a high viscosity fluid (also treated in this paper) other time scales such as the viscous scale $\tau_\eta = \eta R_0/\gamma$ arising from a balance of surface tension and viscosity, might be more appropriate. However, to avoid confusion we will consistently use the inertial-capillary time scale. There still remain three independent dimensionless parameters in the problem. The time scale λ of the polymer is conventionally called a Deborah number, De , when made dimensionless with the characteristic time scale of the system. In the present study we thus have $De = \lambda/\tau$. Note that the Deborah number is ‘intrinsic’ to the fluid thread because it is defined entirely in terms of material and geometric parameters. It does not contain the rate of stretching in the fluid, since the flow is not forced but is free to select its own rate of stretching, which may be spatially and/or temporally inhomogeneous. The other two dimensionless parameters represent the relative contributions of viscous stresses from the solvent and the polymer. There are a number of possible representations for these parameters. The total dynamical viscosity for a dilute polymer solution characterised by the Oldroyd-B model is given by $\eta_0 = \eta_s + \eta_p$ and the relative importance of viscous effects can thus be characterised by the Ohnesorge number $Oh = \eta_0/\sqrt{\rho\gamma R_0}$ (von Ohnesorge (1936)) and the solvent viscosity ratio $S = \eta_s/\eta_0$. An alternative representation which we use below is to separate the relative dimensionless contributions of the kinematic viscosity $\nu_s = OhS$ of the solvent, and the polymeric contribution to the viscosity $\nu_p = Oh(1 - S)$. All these material constants have been made dimensionless using R_0 , γ and τ as the characteristic scales.

It is very difficult to describe the complexity contained in this three-dimensional parameter space in full generality, so in the following we will restrict ourselves to the case of large $De \gg 1$, implying that the non-Newtonian polymer contribution is significant

at all times. Physically this means that De is much larger than the initial time scale of the liquid bridge's evolution, which is set by the linear stability of the fluid thread. At low viscosities, $Oh = \nu_s + \nu_p < 1$, this time scale is $O(1)$ by virtue of the chosen time scale for non-dimensionalization. By contrast, for fluids with large viscosities it is set by $\tau_\eta = \tau/Oh$, and we thus require $De/Oh \gg 1$. Note that with the present scaling, $1/Oh^2$ is the ratio of the external length scale R_0 and the intrinsic scale of the fluid, $\ell_\nu = \eta^2/(\gamma\rho)$.

In the early elastic time regime, $t \ll 1 \ll De$, there is no significant decay of polymer stretching. The fluid thus responds as a neo-Hookean elastic material. This allows the effect of the polymers to be written as a *local* contribution to the pressure, given in terms of the interface shape (i.e. the local accumulated strain) alone. The parameter determining the magnitude of this contribution is the dimensionless elastic modulus of the material $G = \nu_p/De$, which is (up to universal constants) proportional to the polymer *concentration*. Depending on the viscosity, the dynamics of the bridge can be quite complex. In particular, for low viscosities, capillary waves can travel along threads and rebound off drops (Li & Fontelos (2003)). Threads are also shown to support elastic waves.

For $De \gg t \gg 1$, as polymers become sufficiently stretched to counter surface tension forces, the simplified, local system of equations converges to a *stationary* solution, maintained by the stress in the polymers with no possibility of relaxation. This stationary solution, originally found by Entov & Yarin (1984), already exhibits the beads-on-string structure, but with a thread of radius $h_{thread} = (G/2)^{1/3}$ to be computed in section 3.2. The transition of the initial evolution to the “quasi-static” region thus occurs approximately when this radius is reached. The term “quasi-static” refers to the fact that the

solution can only be regarded as stationary on time scales much smaller than the polymer relaxation time.

Indeed, to proceed beyond this stage one has to take the viscoelastic relaxation of the polymer chains into account. The structure of the solution is that of cylindrical filaments which thin at an exponential rate $\exp(-t/3De)$ as a result of the local balance between elasticity and capillarity. The filaments connect an arbitrary distribution of droplets, which approach a static, spherical shape. A similarity solution describes the crossover between the cylindrical thread and the neighbouring droplet. Toward the thread, the solution asymptotes toward a constant thickness, in the direction of the drop it matches onto the spherical shape of the drop.

Our paper is organised as follows: In the next section we develop and motivate the lubrication equations to be used for the remainder of this paper. A numerical simulation illustrates the regimes to be analysed below. The third section is devoted to the study of the neo-Hookean regime, where polymer relaxation can be neglected. The resulting local description of the polymer stresses is tested numerically and then used to compute the asymptotic thread radius. The fourth section deals with the long time regime at finite De for which exponential thinning of threads is observed. After giving a qualitative description of the shape and flow inside the thread, we introduce a similarity description valid in the corner where a cylindrical thread meets a spherical drop. If De is large enough to make only elastic and surface contributions relevant, we can compute all but one of the free parameters of the solution. This last parameter, the thread radius, can be estimated by matching to the early-time regime. The numerical results are compared with experimental observations using a dilute solution of monodisperse polystyrene which is well-described by the Oldroyd-B constitutive model. Measurements of the evolution in the mid-filament radius and the evolution of the spatial profile of the filament are

well-described by the theory. In the final section we discuss work that remains to be done within the framework of the present model, as well as perspectives for inclusion of other effects that lie beyond it.

2. Model and simulation

2.1. One-dimensional equations

In this paper we confine ourselves to the study of a simplified version of the Oldroyd-B model for polymeric liquids, assuming that the radius $h(z, t)$ of the liquid column varies slowly. Thus the variation of hydrodynamic variables inside the column is also small, and we can confine ourselves to the leading order approximation in an expansion in the radius. For example, $v(z, t)$ below is the axial velocity at the centre of the jet. A derivation of the relevant equations has been given in Forest & Wang (1990), so we just give the final result and briefly discuss its physical significance:

$$\frac{\partial h^2}{\partial t} + \frac{\partial}{\partial z} (vh^2) = 0 \quad (2.1)$$

$$\frac{\partial v}{\partial t} + v \frac{\partial v}{\partial z} = -\frac{\partial \kappa}{\partial z} + 3\nu_s \frac{1}{h^2} \frac{\partial}{\partial z} \left(h^2 \frac{\partial v}{\partial z} \right) + \frac{1}{h^2} \frac{\partial}{\partial z} (h^2 (\sigma_{zz} - \sigma_{rr})) \quad (2.2)$$

$$\kappa = \frac{1}{h(1+h_z^2)^{\frac{1}{2}}} - \frac{h_{zz}}{(1+h_z^2)^{\frac{3}{2}}} \quad (2.3)$$

$$\frac{\partial \sigma_{zz}}{\partial t} + v \frac{\partial \sigma_{zz}}{\partial z} = 2 \frac{\partial v}{\partial z} \sigma_{zz} + 2 \frac{\nu_p}{De} \frac{\partial v}{\partial z} - \frac{\sigma_{zz}}{De} \quad (2.4)$$

$$\frac{\partial \sigma_{rr}}{\partial t} + v \frac{\partial \sigma_{rr}}{\partial z} = -\frac{\partial v}{\partial z} \sigma_{rr} - \frac{\nu_p}{De} \frac{\partial v}{\partial z} - \frac{\sigma_{rr}}{De} \quad (2.5)$$

Equation (2.1) expresses volume conservation, (2.2) is the momentum balance equation in the one-dimensional approximation. The first term on the right of (2.2) is the gradient of the Laplace pressure, given in (2.3), which is the main driving force. The rationale behind keeping the full curvature term (2.3) in the leading-order lubrication equations has been discussed in detail in Eggers (1997). Its inclusion guarantees that static spherical

drops are a solution of the equations, so the drops seen in figure 2 can be described in the framework of our lubrication equations.

The second term on the right of (2.2) is the Newtonian contribution to the viscosity, multiplied by the dimensionless viscosity ν_s of the solvent. Finally the last term is the polymeric contribution; σ_{zz} and σ_{rr} are the diagonal terms of the extra stress tensor, with evolution equations given by equations (2.4) and (2.5). The other components of the polymeric stress tensor do not enter at leading order. It is convenient to write all terms on the right-hand-side of (2.2) in the same form, by rewriting the gradient of the mean curvature κ as (Entov & Yarin (1984))

$$\frac{\partial \kappa}{\partial z} = -\frac{1}{h^2} \frac{\partial}{\partial z} (h^2 K \{h\}), \quad (2.6)$$

where we have defined

$$K = \frac{1}{h(1+h_z^2)^{\frac{1}{2}}} + \frac{h_{zz}}{(1+h_z^2)^{\frac{3}{2}}}. \quad (2.7)$$

Notice that K is almost the same expression as κ , but with the sign in front of the second term reversed. Using (2.6), equation (2.2) can finally be rewritten such that the inertial terms on the left are balanced by gradients of the tensile force T in the thread:

$$\frac{\partial v}{\partial t} + v \frac{\partial v}{\partial z} = \frac{1}{\pi h^2} \frac{\partial T}{\partial t} = \frac{1}{h^2} \frac{\partial}{\partial z} \left[h^2 \left(K + 3\nu_s \frac{\partial v}{\partial z} + \sigma_{zz} - \sigma_{rr} \right) \right]. \quad (2.8)$$

The sign of the surface tension contributions to the total tensile force T can be understood by noting that the tension is comprised of ‘bulk’ stresses exerted over the cross-sectional area of the fluid thread, $\pi h^2[-p + 2\nu_s \partial v / \partial z + \sigma_{zz}]$, and a line force exerted around the perimeter, $2\pi h(1+h_z^2)^{-1/2}$. The stress boundary condition on the free surface gives

$$-p - \nu_s \frac{\partial v}{\partial z} + \sigma_{rr} = -\frac{1}{h(1+h_z^2)^{1/2}} + \frac{h_{zz}}{(1+h_z^2)^{3/2}}. \quad (2.9)$$

where the continuity equation has been used to eliminate the radial velocity gradient in

favor of the axial velocity gradient $\partial v/\partial z$. Combining these expressions gives the result in (2.8).

For very viscous fluids the inertial terms on the left of (2.8) are negligible, and the terms in parentheses equal a (generally time-dependent) constant. Alternately, if velocity gradients $\partial v/\partial z$ are small so that the convected derivative terms in (2.4) and (2.5) can be neglected, then these equations describe an additional *Newtonian* contribution ν_p to the total steady-state shear viscosity $\nu = \nu_s + \nu_p$. The presence of polymers also results in fluid viscoelasticity which is represented by the relaxation terms σ_{ij}/De on the right of (2.4) and (2.5). Finally a crucial term for the physics of the following is the first term on the right of (2.4) and (2.5), which describes the interaction of the polymer with the flow. In an extensional flow $\partial v/\partial z$ is positive, so the stress in the axial direction grows as the dumbbells modelling the polymeric contribution to the stress are stretched, while it decays in the radial direction.

2.2. Beads on a string

We are now in a position to study the behaviour of the model for various initial conditions and to compare to experiment. First, we simulate the evolution of a long, initially unstretched cylinder of fluid. For our simulations we have used a numerical code analogous to the one developed earlier by Eggers & Dupont (1994) and Eggers (1997) for Newtonian flows. It is fully implicit and uses adaptive regridding of the numerical mesh to resolve fully the fine structure of the flow. This is crucial to be able to describe some of the last stages of thread formation to be investigated in detail in section 4. We found that the demands on the solution of the implicit equations are much greater than in the Newtonian case, owing to a larger range of time scales in the flow. In general, several iterations of a Newton scheme were necessary for convergence, and significant restrictions had to be put on the time step. To further test for possible problems inherent in our nu-

merical scheme, another *explicit* code was also developed independently. In addition, all fields were represented in a uniform grid, as opposed to the staggered grid of the implicit code. One stability condition for an explicit method is that the time steps Δt must be less than the viscous diffusion time h^2/ν . The explicit method performed quite well except for the highest viscosities, where the time step imposed by the stability condition became prohibitively small.

Figures 3 and 4 give an idea of the typical behaviour of a liquid filament in the absence of gravity, described by (2.1-2.5). The parameters were chosen to be identical to those of figure 2 in Chang et al. (1999); that is in the present scaling, $\nu_s = 0.79$, $\nu_p = 2.37$, and $De = 94.9$, and the amplitude of the initial sinusoidal perturbation is 0.05. The results are quite insensitive to the choice of this amplitude, except that for smaller disturbance amplitudes (as in figure 1 of Li & Fontelos (2003)), the disturbance takes longer to grow to an appreciable size. The left and right hand parts of the picture were produced with the explicit and implicit codes, respectively. Even a blow-up of the corner region at the latest time, where the radius of the filament has fallen below 10^{-2} , does not reveal a significant difference between the results of the two simulations. The same quality of agreement is born out by a comparison of the minimum radius, figure 4.

In figure 4 the minimum radius is initially seen to decrease quite rapidly. Most of this initial motion is described quite well by linear theory (see Chang et al. (1999)). At around $t = 30$ (corresponding to the formation of a filament in the second panel of figure 3), the motion crosses over to a slow exponential decay of the thread radius. This crossover occurs when the elastic stresses which build up in the deforming liquid bridge become dominant and a local elasto-capillary balance is established. The slope drawn into figure 4 corresponds to the theoretical prediction of section 4. During the exponential thinning,

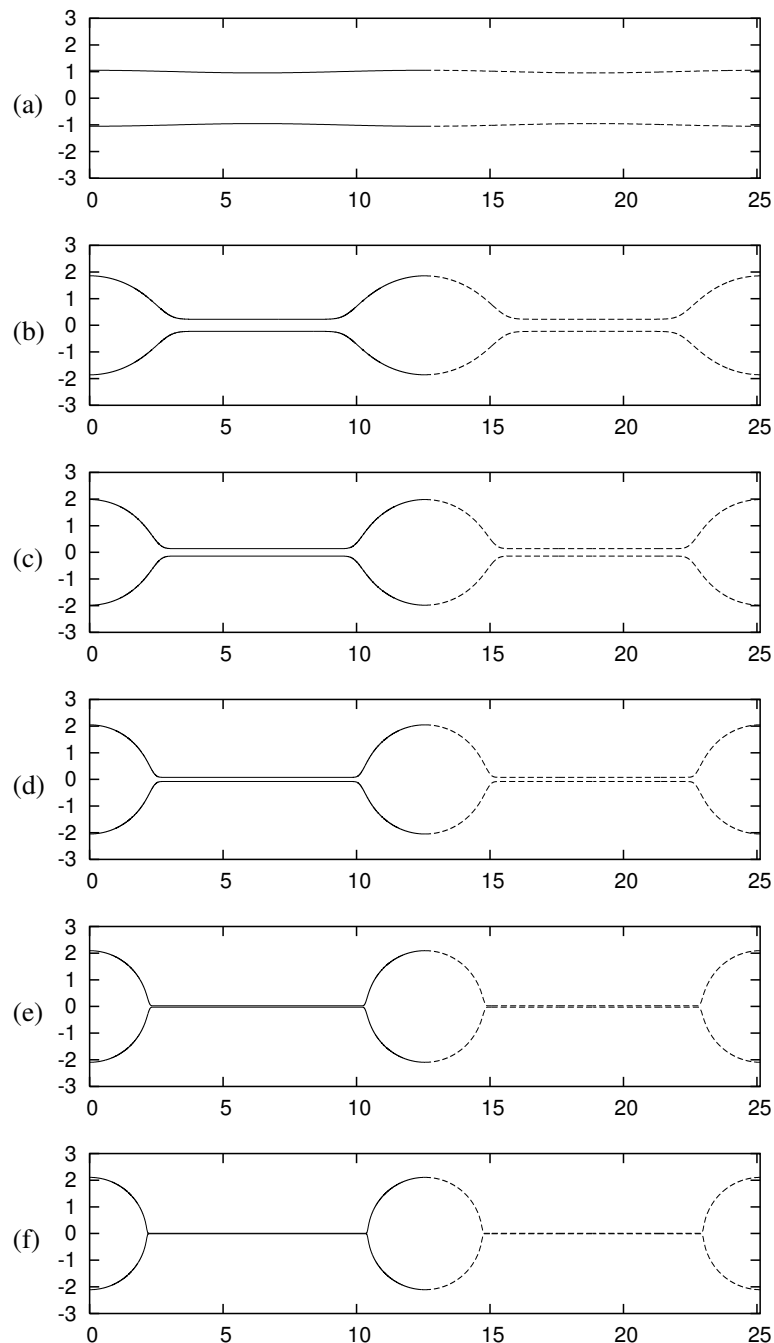


FIGURE 3. A typical series of profiles with periodic boundary conditions and period $L = 4\pi$. The dimensionless parameters are $\nu_s = 0.79$, $\nu_p = 2.37$, and $De = 94.9$. A sinusoidal perturbation of amplitude 0.05 was added in order to make the filament collapse. After the rapid formation of the beads-on-string structure, one observes the slow thinning of the thread. The relative dimensionless times of each profile are (a) 0.0, (b) 31.6, (c) 158.1, (d) 316.2, (e) 632.5 and (f) 948.7. The left-hand-side of the graph (full lines) was produced using the explicit code, the right-hand-side using the implicit code with staggered grid.

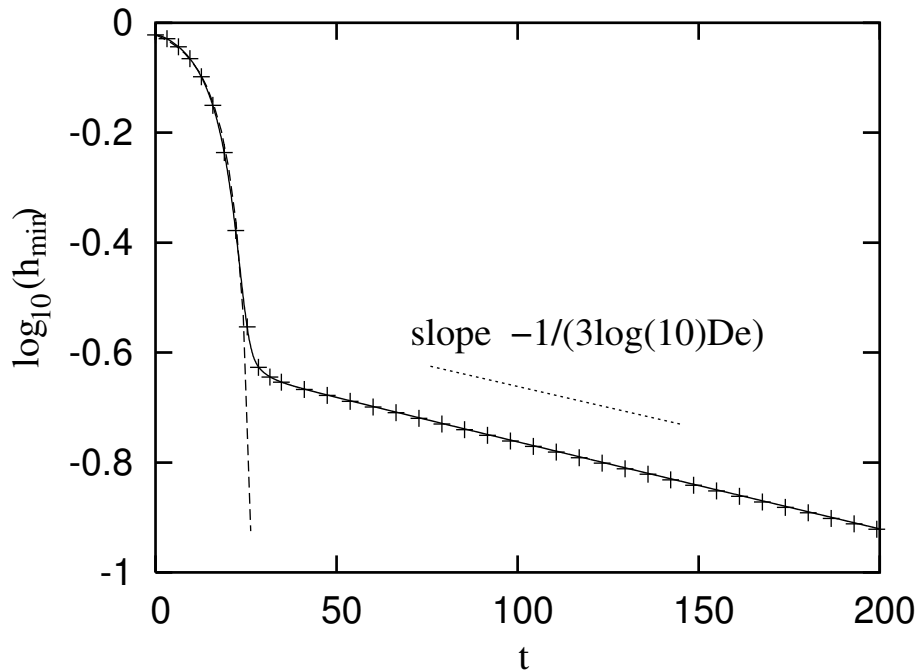


FIGURE 4. The minimum radius corresponding to the profiles shown in figure 3, obtained from the explicit code. One clearly observes a rapid initial motion, which persists until the polymers are appreciably stretched, followed by an exponential thinning at a (dimensionless) rate of $1/(3De)$. Most of the initial motion is well described by linear theory, giving $h_{min} = 1 - A \exp(\omega t)$, where $A = 0.05$ and $\omega = 0.109$. The crosses are the result of our implicit code, which produced the right-hand-side of figure 3.

fluid is expelled from the thread into the surrounding beads, which become increasingly spherical.

Structures very similar to figure 3 are shown in the experiment of figure 2 and have also been observed by Goldin et al. (1969), Bazilevskii et al. (1981), and Christanti & Walker (2001) for the decay of a liquid jet of polymer solution ejected from a nozzle. Good agreement between a numerical simulation of a one-dimensional model very similar to ours and the experiments of Bazilevskii et al. (1981) has been reported by Yarin

(1993), p.85. However, it is very difficult in practise to produce liquid cylinders without stretching the polymers, since there is considerable shear inside the capillary tube and the nozzle. On the other hand, the shear flow inside the capillary is very difficult to model in the framework of the present one-dimensional description. Furthermore, each bead and ligament shown in figure 2 corresponds to a ‘snapshot’ at a different elapsed convective time $\Delta\tilde{t} = L_{period}/v_{jet}$. Therefore, to compare quantitatively to experiments, we prefer to use a setup that allows for a more quantitative description of the stretching history of the fluid column.

2.3. Liquid bridge

We now turn to the capillary thinning and breakup of a liquid bridge that has been subject to a very rapid initial stretching. During this extensional step strain process (which typically lasts 0.05 sec) hardly any polymer relaxation takes place and, provided that the initial aspect ratio is not too small, the exact temporal profile in which the the plates are pulled apart is not very important. In fact, the initial stretching is well described by a simple model neglecting any spatial structure (Anna & McKinley (2001)). However, the simulation within the one-dimensional model is somewhat subtle, owing to a difficulty in imposing the boundary conditions at the end-plates. Namely, the no-slip boundary condition enforces a vanishing tangential velocity at the end-plate, and consequently $\partial v/\partial z = 0$, while this is not true in the one-dimensional model. Since the stretch rate $\partial v/\partial z$ is in fact large over most of the bridge, this creates a thin boundary layer of fully three-dimensional flow near the end-plates. Failure to correctly implement this boundary layer leads to a detachment of the interface from the ends within the lubrication model. Following Stokes et al. (2000), we have avoided this problem by introducing a supplementary viscosity which strongly increases near the ends. This position-dependent viscosity

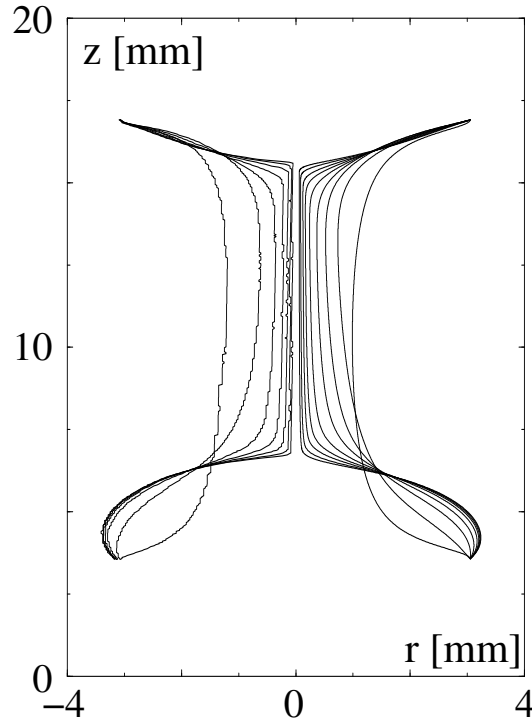


FIGURE 5. A comparison between experimental profiles (left), obtained from digitising the images of figure 1 and corresponding simulations (right), including the initial stretching and gravity (acting downward). The time difference between two consecutive images is 10 sec. The reduced variables corresponding to the experimental parameters are $\nu_s = 193.2$, $\nu_p = 29.04$, and $De = 296$. Note that there are *more* profiles from simulation to reach approximately the same thread radius, corresponding to a slight overestimation of the experimental time scale.

has been constructed by matching to a three-dimensional squeeze flow near a solid wall.

The effective “freezing” of the fluid prevents any lateral slip along the bounding wall.

When the initial aspect ratio of the liquid bridge is small $\Lambda_0 = L_0/R_0 \ll 1$ there is an additional consequence of the no-slip boundary condition. Numerical simulations show that there is an additional stretching of material elements near the free surface associated with the strong radial inflow and this can introduce a radial variation in the elastic stress

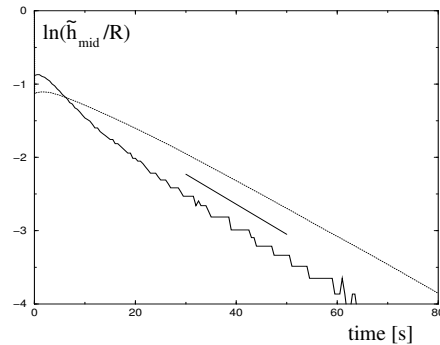


FIGURE 6. The logarithm of the normalised minimum radius corresponding to the experimental (circles) and theoretical (dotted line) profiles of figure 5. The thick line is the theoretical prediction for the slope $-1/(3De)$.

near the centerplane of the filament (Harlen (1996)). This additional elastic stress can be incorporated into a slender filament theory if desired; for example by assuming a specific power law form for the radial variation in the axial polymeric stress (Kolte & Szabo (1999)). However, numerical simulations (Yao & McKinley (1998)) show that this effect is negligible for liquid bridges with $O(1)$ aspect ratios as used in the present work and we do not consider this effect further.

Figures 5 and 6 allow for a direct comparison between simulation and experiment. The first digitised profile is taken just after cessation of stretching, after that a profile is shown every 10 sec. Theory and experiment show good agreement in all the basic features of the flow, such as the sagging under gravity and the formation of the thread. Two subtle differences can be seen: first, the timescale of the simulation is off by about 20%, so 9 experimental profiles are shown but only 7 theoretical ones, at which point about the same minimum thread radius is reached. This discrepancy, also seen in figure

6, is quite acceptable considering that no adjustable parameters were introduced. Most of the difference stems from the early-time development when two-dimensional effects may be significant (Harlen (1996), Yao & McKinley (1998)), whereas the asymptotic slope of both simulation and experiment agrees well with the theoretical prediction.

The behaviour of h_{min} at early times is markedly different from that of a free jet, as discussed in detail in Anna & McKinley (2001). The rapid early decrease of h_{min} seen in figure 4 is absent, since stresses are already large owing to the initial stretching of the liquid bridge. On the contrary, some of this initial stress has to relax before further thinning can start, as seen in the plateau for the earliest times. Evidently there are some subtle features of the experimental relaxation processes which are not modelled correctly by our single-mode Oldroyd-B model. The initial stretch is also responsible for the absence of drops (“beads”) in the middle of the thread that formed on the free jet, cf. figure 3. The reason is that the initial stretch is uniform, and this uniformity is conserved by the exponential stretching regime.

The second difference between the experimental and theoretical profiles of figure 5 is that at the same minimum thread radius the corner between the thread and drops at the end is *sharper*. We will return to this when we discuss the structure of the corner region in detail in section 4.2.

3. Early time asymptotics

3.1. Local description

In this section we exploit the fact (Entov & Yarin (1984), Fontelos (2003)) that for early times $t \ll De$ the non-Newtonian contribution to the stress behaves like that of a neo-Hookean elastic solid, and can be expressed directly through the profile shape $h(z)$. The

elastic modulus of the material is related to the model parameters by

$$G = \nu_p / De. \quad (3.1)$$

With the present scaling this is the same as the *elastocapillary* number introduced in Anna & McKinley (2001), which can also be written $G = Oh(1 - S)/De$.

Using Lagrangian coordinates, Fontelos (2003) shows that the polymeric stress appearing in (2.8) can be written as

$$h^2 (\sigma_{zz} - \sigma_{rr}) = G (1/h^2 - h^4) + O(t/De), \quad (3.2)$$

where we used that throughout this paper $R_0 = 1$. The exact form of the correction terms can be found in (Fontelos (2003)). Thus in the neo-Hookean limit the equation for the velocity is

$$\frac{\partial v}{\partial t} + v \frac{\partial v}{\partial z} = \frac{1}{h^2} \frac{\partial}{\partial z} \left(h^2 K + 3\nu_s h^2 \frac{\partial v}{\partial z} + G (1/h^2 - h^4) \right), \quad (3.3)$$

where K is defined in (2.6).

As a numerical test of the quality of the local approximation, we performed two simulations similar to that of figure 3, but for two different *Deborah* numbers. figure 7 shows the evolution of the interface profile at different times for $De = 94.9$, $\nu_p = 2.37$ (left column), and $De = 9490$, $\nu_p = 237$ (right column). The full lines are the solution of equations (2.1-2.5), while the dashed ones were obtained by replacing (2.2) by (3.3). For the simulation corresponding to moderate Deborah number, the time t of the second panel is of same order as the relaxation time De , so the solution of the full equations and the one of the local approximation begin to differ starting from the third panel. On the other hand, for the case of large Deborah number, $t \ll De$, throughout the simulation the agreement of the two solutions is excellent.

Throughout the process of filament formation, we find almost perfect agreement with the local model provided $De \gg t$. Thus the local approximation is an extremely use-

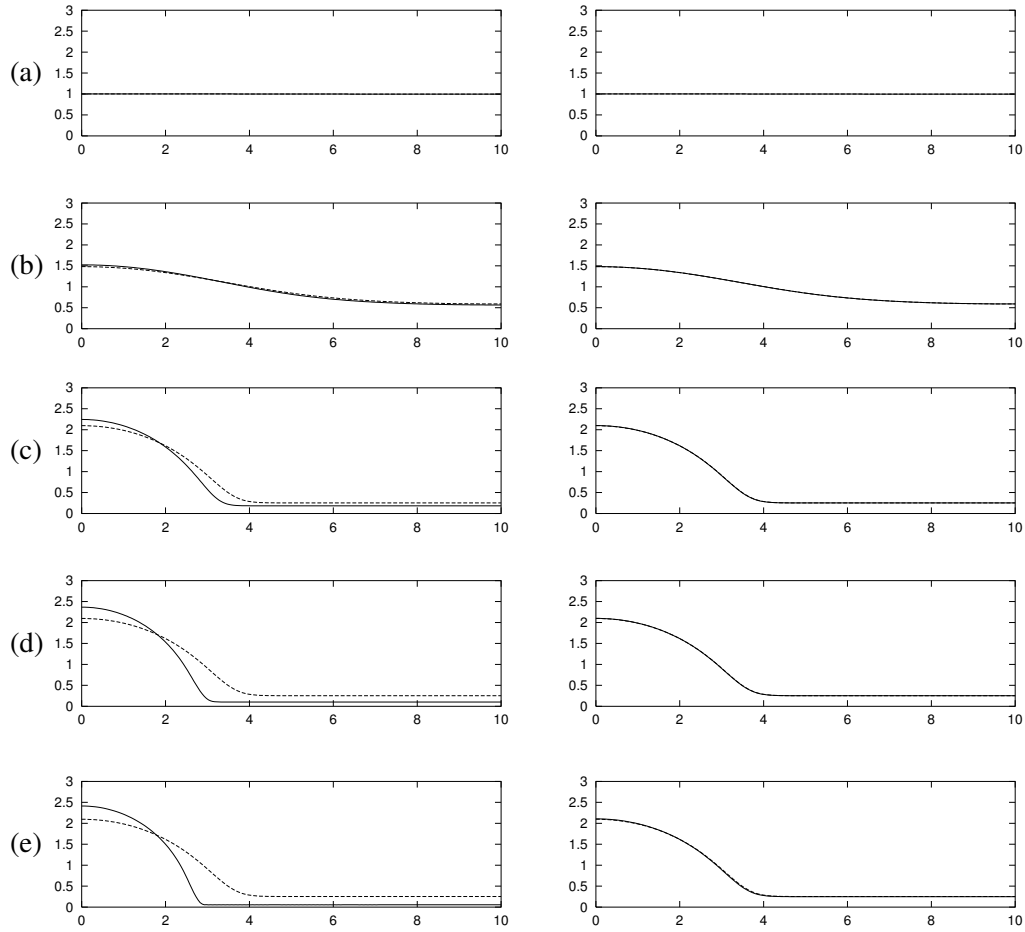


FIGURE 7. Comparison of interface profiles with period $L = 20$ and $\nu_s = 0.79$ between the full equations (full) and the local approximation (dashed lines): left column $De = 94.9$ and $\nu_p = 2.37$, and right column $De = 9490$ and $\nu_p = 237$. The relative times for each profile are (a) 31.6, (b) 79.1, (c) 158.1, (d) 316.2 and (e) 474.3. Evidently, for $t \ll De$ the agreement is excellent (right column).

ful tool to investigate the early-time dynamics $t < De$ and the formation of the basic beads-on-string structure. We will therefore study the stationary filament solutions of the local model in the following subsection. After the filament has formed, the neo-Hookean elastic response of the local model leads to a stationary profile, while the effects of fluid

viscoelasticity captured by the full equations leads to the filament continuing to thin exponentially in time.

At low viscosities, $Oh < 1$, the initial evolution can be considerably more complicated, but is still fully described by the local equations if De is sufficiently large. This is due to inertial effects also being important; so as the thread is formed, fluid may rebound from the drops, and an additional ‘secondary’ drop forms in the middle of the filament. This is also seen in experimental observations of jet breakup (Christanti & Walker (2001)) and drop pinch-off (Cooper-White et al. (2002)).

3.2. Static solutions

In the neo-Hookean limit considered here, $De \rightarrow \infty$, the elastic stresses never relax, so at long times surface tension is balanced by permanent elastic stresses to form a stationary solution. Integrating (3.3) while dropping inertial terms, one finds

$$h^2 K + G(1/h^2 - h^4) = T, \quad (3.4)$$

where T is the unknown tension in the string. Apart from the appropriate boundary conditions on h , (3.4) has to be solved with the constraint of volume conservation

$$\pi \int_0^L h^2 = V, \quad (3.5)$$

which only serves to set the size of the fluid drops.

In particular, (3.4) allows for solutions with constant h

$$h_{thread} + G/h_{thread}^2 = T, \quad (3.6)$$

where we have assumed a constant initial radius $R_0 = 1$, and dropped the contribution from the radial stress, since h_{thread} is expected to be small. The solutions of equation (3.6) correspond to the thin cylindrical thread of constant radius shown schematically in figure 8. Indeed, from the balance (3.6) one concludes that both T and h_{thread} scale like

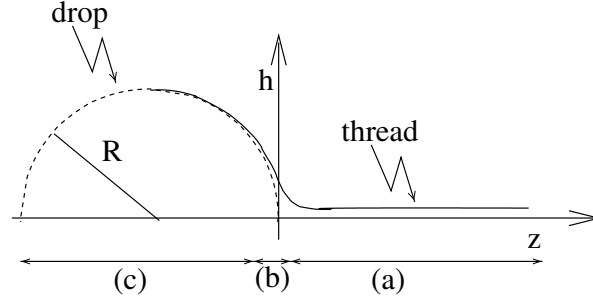


FIGURE 8. A schematic of a thread connected to a drop. The origin $z = 0$ is placed at the end of the spherical drop.

$G^{1/3}$, which is small for large De . The thread has to be matched to an almost circular drop, as first done by Entov & Yarin (1984), and illustrated in figure 8.

In the drop region the radius h is of order one and in (3.4) one can neglect the tension T and the terms multiplied by G in the limit we are interested in. Thus one is left with the contribution from surface tension alone, and the solution is a spherical drop (region (c) of figure 8),

$$h(z) = R\sqrt{1 - (1 + z/R)^2}. \quad (3.7)$$

Here R is the radius of the drop. Since in the asymptotic limit there is very little fluid inside the thread, R is set by the volume constraint (3.5).

To determine h_{thread} , one needs the value of the constant T , which requires matching the thread (region (a)) to the drop (region (c)). One can avoid considering the connecting region (b) by computing a first integral of (3.4), multiplying the equation by h'/h^3 and using

$$\left(\frac{1}{h(1 + h_z^2)^{1/2}} \right)' = -\frac{h_z}{h^2(1 + h_z^2)^{1/2}} - \frac{h_z h_{zz}}{h(1 + h_z^2)^{3/2}}. \quad (3.8)$$

This gives

$$\frac{1}{h(1+h_z^2)^{1/2}} + \frac{G}{4h^4} + \frac{Gh^2}{2} = \frac{T}{2h^2} + \frac{1}{\bar{R}}, \quad (3.9)$$

where the constant of integration $1/\bar{R}$ is essentially half the Laplace pressure inside the spherical drop (remembering that the coefficient of surface tension has been normalized to one). Indeed, evaluating (3.9) on top of the drop, where h_z is zero, one finds $\bar{R} \approx R$, since T goes to zero in the limit of vanishing G . In the thread h_z vanishes as well, giving

$$1/h_{thread} + G/(4h_{thread}^4) = T/(2h_{thread}^2) + 1/\bar{R}, \quad (3.10)$$

again dropping radial contributions which are very small in the thread. In deriving (3.10) we have also assumed that (3.4) is valid everywhere including the drop, the cylindrical thread *and* the corner region. If additional terms beyond the one-dimensional approximation are important in the corner region this will affect the value of \bar{R} .

Remembering our previous estimate $h_{thread} \propto T \propto G^{1/3}$, the constant $1/\bar{R}$ is *subdominant* in (3.10), and thus combining (3.10) with (3.6), we find

$$h_{thread} = \left(\frac{G}{2}\right)^{1/3}. \quad (3.11)$$

For the parameters of figure 7 (right column), we find $h_{thread} = 0.232$ from (3.11), to be compared with the observed value of $h_{min} = 0.253$. The quality of the approximation quickly improves as the scale separation between thread thickness and drop size becomes even more complete.

4. Late time asymptotics

4.1. Thread thinning

The formation of threads described in the previous section is a result of the interplay of surface tension and elastic forces. On times longer than De however the string tension gradually relaxes, and the thread thins at an exponential rate β . This rate is easily

determined from a balance of surface tension and elastic forces in (2.2), assuming a spatially constant profile (e.g. Bazilevskii et al. (1981), Renardy (1995), Entov & Hinch (1997))

$$h(z, t) = h_0 \exp(-\beta t). \quad (4.1)$$

From volume conservation (2.1) one finds that the extension rate $\partial v/\partial z = 2\beta$ in the thread is constant. The exponential growth of the axial stress σ_{zz} is described by (2.4), and assuming a spatially constant σ_{zz} one immediately finds $\sigma_{zz}(z, t) = \sigma_0 \exp[(4\beta - 1/De)t]$. The radial stress σ_{rr} decreases exponentially and does not figure in the balance. Remembering that capillary pressure is balanced with σ_{zz} in (2.2) and rewriting the pressure gradient according to (2.6) one finds

$$h + h^2 \sigma_{zz} = T(t), \quad (4.2)$$

for the tension $T(t)$ in the string, performing one spatial integration. For the balance (4.2) to be consistent σ_{zz} must grow like $1/h$, and thus $\beta = 1/(3De)$, implying that the tension itself decays like

$$T = a_1 \exp[-t/(3De)], \quad (4.3)$$

and

$$\sigma_{zz}(z, t) = \sigma_0 \exp(t/De). \quad (4.4)$$

The fact that $\beta = 1/(3De)$ means that the thinning rate of the thread given by (4.1) is directly related to the time scale of the polymer, providing for a convenient experimental probe. Furthermore the tensile force T in the thinning thread is not identically zero as assumed in earlier work (Entov & Hinch (1997)) but in fact decays as the same rate as the radius.

To obtain a clearer physical picture, we plot in figure 9 the thread radius, normalised

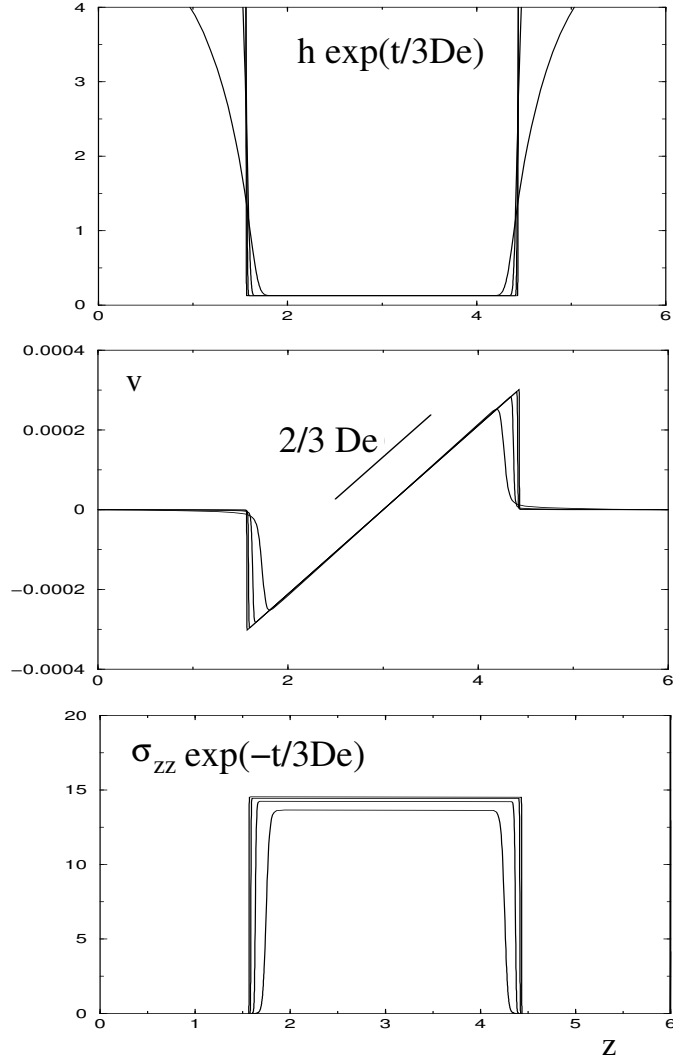


FIGURE 9. Profiles of the radius, the velocity, and the axial stress, normalised by their values in the thread, in the regime of exponential thinning. The parameters are $De = 3164$ and $\nu_s = \nu_p = 95.6$. The extension rate inside the thread is $2/(3De)$.

by the exponential factor $\ell = \exp[-t/3De]$, the velocity in the thread, and $\ell\sigma_{zz}$ for a number of different times during the thinning. As predicted, $h(z)$ and $\sigma(z)$ are very nearly constant over the thread, and they collapse nicely as anticipated by the above scaling laws. Furthermore, the extension rate $\partial_z v$ has the constant positive value 2β inside the

thread, expressing the fact that fluid is expelled from it. In response, the stress σ_{zz} grows to large *positive* values, so both contributions on the left-hand side of (4.2) are always positive. This means that the tension T (which below we will compute explicitly in the limit of large De) has to be kept in (4.2) for a consistent balance. For large De this makes the stress twice as large as determined in earlier work (e.g. Bazilevskii et al. (1981), Entov & Hinch (1997), Anna & McKinley (2001)), where the tension was not considered.

Since the total length L of the thread is a constant quantity, the maximum value of the velocity

$$v_{max} \approx \frac{L}{3De} \quad (4.5)$$

behaves like the inverse of the Deborah number, and is thus small in the limit that is the chief focus of this paper. A number of experiments (e.g. Bazilevskii et al. (1997), Stelter et al. (2000), Anna & McKinley (2001)) have confirmed the prediction (4.1). In particular in Anna & McKinley (2001) the relaxation time was determined independently, and the thinning rate was found to conform with the prediction $\beta = 1/(3De)$. At both ends of the thread, the velocity and the stress fall to zero very sharply, and the profile merges onto a static drop with radius R . Next we will focus on this transition region, whose scale is set by $\ell = \exp(-t/3De)$.

4.2. *The corner region*

According to the scalings found in the previous subsection, which implies the existence of a small length scale $\ell = \exp(-t/3De)$, it is natural to look for solutions of (2.1-2.2) of the form

$$\begin{aligned} h(z, t) &= \ell \bar{h}(\bar{z}, t) \\ v(z, t) &= \bar{v}(\bar{z}, t) \end{aligned} \quad (4.6)$$

$$\sigma_{zz}(z, t) = \ell^{-1} \bar{\sigma}_{zz}(\bar{z}, t),$$

where $\bar{z} = \ell^{-1}(z - z_0)$. The origin z_0 must asymptotically lie in the similarity region. A convenient choice is the position of the extremum of the velocity in the limit $\ell \rightarrow 0$. Since σ_{rr} is exponentially small inside the thread, it can be left out of our analysis. Thus the equations for \bar{h} , \bar{v} , and $\bar{\sigma}_{zz}$ are

$$\begin{aligned} 2\ell\bar{h}\dot{\bar{h}} - \frac{2\ell}{3De} \left(\bar{h}^2 - \bar{z}\bar{h}\bar{h}' \right) + \left[\bar{v}\bar{h}^2 \right]' &= 0 \\ \bar{h}^2 \left(\ell^2\dot{\bar{v}} + \frac{\ell^2\bar{z}}{3De}\bar{v}' + \ell\bar{v}\bar{v}' \right) &= \left[\bar{h}^2 K\{\bar{h}\} + \bar{h}^2(3\nu_s\bar{v}' + \bar{\sigma}_{zz}) \right]' \\ \ell\dot{\bar{\sigma}}_{zz} + \frac{\ell}{3De}(\bar{\sigma}_{zz} + \bar{z}\bar{\sigma}'_{zz}) + \bar{v}^3 \left[\frac{\bar{\sigma}_{zz}}{\bar{v}^2} \right]' &= \frac{\ell}{De}(2\nu_p\bar{v}' - \bar{\sigma}_{zz}), \end{aligned} \quad (4.7)$$

where the prime refers to differentiation with respect to the similarity variable \bar{z} and the overdot indicates differentiation with respect to time. Towards the thread our scaling ensures that \bar{h} , \bar{v} , and $\bar{\sigma}_{zz}$ tend toward the constants h_0 , v_0 , and σ_0 , respectively, as $\bar{z} \rightarrow \infty$. (Without loss of generality, we assume that the thread is to the right of the transition region.) The length scale ℓ becomes exponentially small for $t \rightarrow \infty$ and for any finite \bar{z} , terms proportional to ℓ or ℓ^2 may be dropped. Looking for time-independent solutions of (4.7) and integrating once, we find

$$\begin{aligned} \bar{v}\bar{h}^2 &= v_0 h_0^2 \\ \bar{h}^2 K\{\bar{h}\} + \bar{h}^2(3\nu_s\bar{v}' + \bar{\sigma}_{zz}) &= h_0 + h_0^2\sigma_0 \\ \bar{\sigma}_{zz}/\bar{v}^2 &= \sigma_0/v_0^2. \end{aligned} \quad (4.8)$$

Eliminating \bar{v} and $\bar{\sigma}_{zz}$, we end up with

$$\bar{h}^2 K\{\bar{h}\} + \bar{h}^2(-a_2\bar{h}'/\bar{h}^3 + a_3/\bar{h}^4) = a_1, \quad (4.9)$$

where $a_1 = h_0 + h_0^2\sigma_0$, $a_2 = 6\nu_s v_0 h_0^2$, and $a_3 = \sigma_0 h_0^4$. In our analysis of (4.9), we are

going to confine ourselves to the limit of very large De , for which typical velocities are small, according to (4.5). Thus the contribution $-a_2\bar{h}'/\bar{h}$ in (4.9), which comes from the viscous stress, can be neglected. Dropping this term makes (4.9) equivalent to (3.6), so our previous asymptotic analysis can be applied to calculate the minimum thread radius. Just as in section 3, the dominant balance inside the drop is $0 = K\{\bar{h}\} = K\{h\}$, which is the equation for a static drop described by (3.7). Thus (4.9) is valid not only in the self-similar region described by (4.6), but all the way into the drop. Using the results of section 3, we find

$$\sigma_0 = 2/h_0, \quad a_1 = 3h_0. \quad (4.10)$$

These expressions can be combined with (4.4) to evaluate the exponential growth in the extensional stress, once the amplitude h_0 of the thread radius is determined. The thread radius (and thus h_0) is readily measurable by optical means; thus giving experimental access to the growth in the polymeric stress, which is difficult to obtain by other means. Below we also provide an estimate of h_0 by matching 4.1 to the initial thinning of the jet. Renardy (1995) also computes the constant a_1 , but without resolving the self-similar corner region, as we do. He does not include the full curvature in his description, and is thus unable to describe the drop. Instead, the transition to the drop is described as a shock, and the estimate for a_1 becomes $3/2h_0$, half of the value we find.

In the limit of small thread radius the first integral of (4.9), analogous to (3.9), is

$$\bar{h}' = - \left[\frac{4(\bar{h}/h_0)^2}{(3 - (h_0/\bar{h})^2)^2} - 1 \right]^{1/2}. \quad (4.11)$$

As in the previous section we are assuming here that our slender filament equations apply uniformly in the bead, the cylindrical filament and the matching region.

Integrating (4.11) with initial radius $\bar{h} = h_0$ (plus an arbitrarily small perturbation) one finds the universal profile shape of $\bar{h}(\bar{z})$. In figure 10 we show the corner region of the

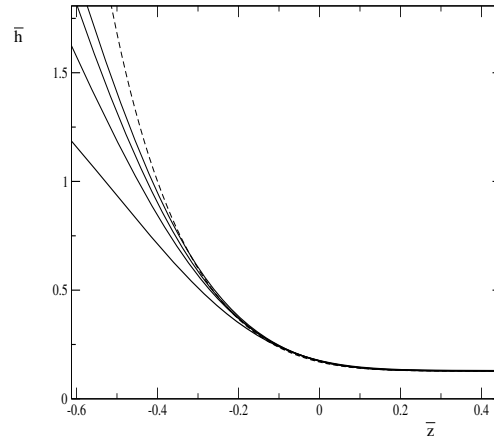


FIGURE 10. A comparison of our similarity theory for large De (dashed line) with rescaled profiles from a numerical simulation with parameters as in figure 9, at $\log_{10}(h_{min}) = -1.5, -2, -2.5,$ and -3 . The dashed line was obtained from integrating (4.11), with $h_0 = 0.1275$.

numerically computed profiles presented in the top panel of figure 9, rescaled according to (4.6) (solid lines). Using the value of $h_0 = 0.1275$ read off from figure 9, the dashed line is obtained by integrating (4.11). As t grows, the rescaled profiles converge nicely to the theoretical prediction.

Finally, we compare our theoretical results to experiments. To that end, high resolution images of experimental profiles were taken by focusing a video microscope on the corner region. Figure 11 shows a sequence of digitized images of the upper corner, which becomes increasingly sharp as the thread thins. To test our similarity theory, the profiles corresponding to the latest stages of pinching were rescaled using the minimum thread radius for both axes. As shown in figure 12, the experimental profiles converge nicely onto a master curve, in very much the same way as the computed profiles of figure 10 do. However, the experimental profiles turn out to be *sharper* than theory predicts, a fact we attribute to the failure of the one-dimensional equations underlying our theory. This point is discussed in more detail below.

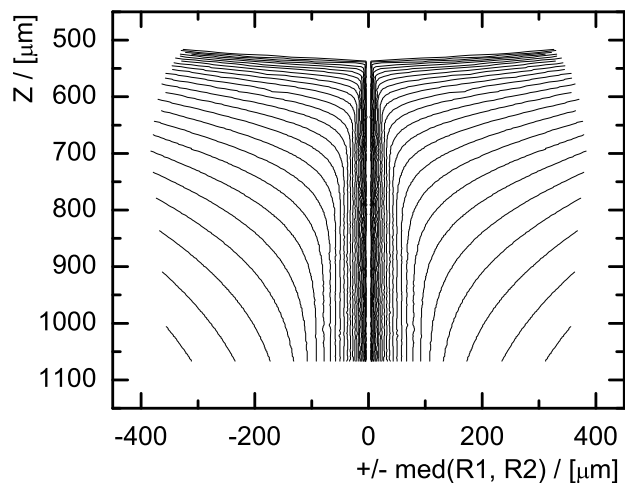


FIGURE 11. An experimental closeup of the upper corner of the liquid bridge. Shown is the same experiment as figure 1, but under a microscope. The time interval between two consecutive profiles is 2 *sec*.

The constant h_0 is the only remaining adjustable parameter for the description of the corner region. In the case of the free jet, cf. section 2.2, it can in fact also be estimated in the limit that the relaxation time De of the polymer is much larger than the time t_{fil} needed to form the primary filament. Namely, equating the thread thickness (3.11) given by the local theory of section 3 with $h_{min} = h_0 \exp(-t_{fil}/3De)$ one finds

$$h_0 = \exp(t_{fil}/(3De)) \left(\frac{G}{2}\right)^{1/3}.$$

Thus in the limit that De is much larger than t_{fil} one simply has

$$h_{min}(t) = \left(\frac{G}{2}\right)^{1/3} \exp(-t/3De), \quad (4.12)$$

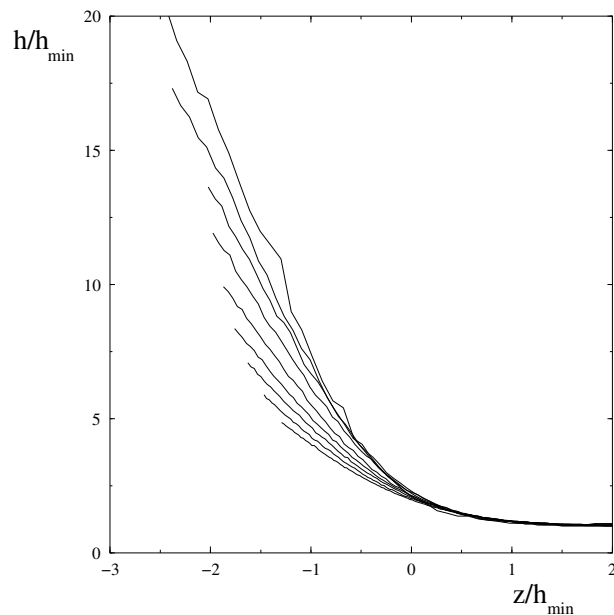


FIGURE 12. The last 9 experimental profiles (corresponding to figure 11), taken in time intervals of 0.5 sec, with both axes rescaled by the minimum thread radius.

which is smaller by a factor of $2^{-1/3}$ than the result given in Bazilevskii et al. (1997) and Entov & Hinch (1997), which do not take into account the tension in the string. Fitting a straight line to the exponential thinning regime of figure 4, we obtain $h_0 = 0.247$, in excellent agreement with the theoretical prediction of (4.12), $h_0 = (G/2)^{1/3} = 0.232$.

5. Discussion

By confining ourselves to the simplest possible model for a dilute polymer solution, we have reached in the present paper at a rather complete description of the formation and subsequent development of the beads-on-string structure. Some details, of course, remain to be elaborated.

At low viscosities or high surface tension, $Oh \ll 1 \ll De$, Li & Fontelos (2003) show that a complex succession of beads may be generated owing to inertial effects. Namely,

originating from the drop, a capillary-elastic wave propagates along the neck to form a thin thread of uniform thickness. At places where the wavefronts meet, smaller satellite drops form. After a sequence of drops has formed, these drops are subject to possible merging, or draining processes.

A superficially similar, yet physically quite distinct phenomenon has been described in Chang et al. (1999) and named ‘recoil’. By this the authors refer to the instability of exponentially thinning threads of constant thickness, originating from the drop. As a result, a secondary, thinner thread forms on the primary one. We never found any indication of secondary filament formation after an exponentially thinning thread was formed, either in simulation or in experiments with highly viscous polymer solutions. We also repeated the simulations of Chang et al. (1999) for the same parameter values, using both our explicit and implicit codes. In our simulations, the primary thread continued to thin, without any indication of secondary thread formation. It would be interesting in the future to investigate the possibility of instabilities being generated by noise of *finite* amplitude.

As indicated above, the velocity in the corner region is proportional to $1/De$, thus in the limit of large De , viscous effects drop out and only capillary and elastic forces remain. In the presence of viscous forces, equation (4.9) can be applied for any finite value of the similarity variable \bar{z} . However, we have not yet succeeded in matching the solution described by (4.9) with the stationary drop in the general case. The reason is that whilst in the similarity region close to the corner (between the thread and the drop) everything can be described by the thread profile \bar{h} alone, this is no longer possible in the transition region toward the stationary drop. Instead, the coupled system involving the drop shape, the velocity field, and the stress has to be treated. Indeed, even in the

limit of large De where matching can be achieved using h alone, analytical computation of v and σ_{zz} is far from trivial.

A result of the present similarity description is that for very long times the drop develops into a perfect sphere, while the thread radius shrinks to zero. This means the profile at the point where the thread meets the drop develops into a right angle. Unfortunately, the fact that the slope of the profile becomes increasingly large in the corner means that the lubrication equations, used throughout this paper, are no longer valid. However, a preliminary investigation suggests that in fact the full three-dimensional, axisymmetric Oldroyd B equation leads to the same self-similar scaling as the lubrication model (Eggers et al. (2005)). The resulting similarity equations are, however, much more complicated, and require numerical methods to solve. We are currently developing a boundary integral method to treat the similarity equations, whose solution we hope to compare to experiment (Eggers et al. (2005)).

Finally, there are myriad effects associated with departures from the Oldroyd-B model, some of which have already been incorporated into the description of thread thinning. For example, the effect of the finite extensibility of a real polymer chain will change the dynamics, since it bounds the maximum elastic stress that can be exerted by the polymer chain (Entov & Hinch (1997)). This is modelled theoretically by the presence of nonlinear terms in the constitutive equation for the polymeric stresses, which limit their growth. Thus, whereas the exponential thinning described in this paper would formally lead to breakup only in infinite time, a real polymer thread does in fact break. Experimental observations of the departure from the exponential law are found for example in Bazilevskii et al. (1997) and Anna & McKinley (2001). The theory in Bazilevskii et al. (1997) differs from the conventional one in that it credits the *degradation* of polymers for the departure from the exponential law.

A number of different nonlinear constitutive equations which bound the maximum polymeric stress have been proposed, and Renardy (Renardy (2001), Renardy (2002)) has considered the asymptotics of a number of different models. A key feature of these analyses is that the thread is predicted to break in finite time when the maximum elastic stress, arising from affine deformation can no longer balance the capillary pressure γ/\tilde{h}_{min} . For dilute polymer solutions in particular, the nonlinear form of the force-extension curve close to full extension is well-established both experimentally and theoretically (Li et al. (2000), Shaqfeh et al. (2003)). Analysis of extensional flow of finitely extensible nonlinear elastic (FENE) dumbbells results in a maximum (dimensionless) polymeric stress of order $\sigma_{zz,max} \approx (2De)Gbv'$ where $b = 3N_K$ is the finite extensibility parameter, which is proportional to the number of Kuhn steps or links (N_K) in the polymer chain. In the elastocapillary necking regime we obtain $(2De)v' = 2/3$ (cf. figure 9); a naive balance thus suggests that we require $Gb > 2/3$ for elastic effects to be able to grow sufficiently large to balance capillary stresses. A rigorous balance is substantially more complex (Entov & Hinch (1997)) and requires a consideration of the initial polymeric stress in the filament and the additional strain accumulated by the fluid in the transient process of the polymeric stress growing to the saturation value $\sigma_{zz,max}$. Numerical calculations show that the time to breakup depends on the specific functional form of the chosen constitutive model (Harlen (1996), Yao & McKinley (1998), Fontelos & Li (2004)).

Other, more elaborate versions of the FENE model have also been developed (Lhuillier (2001), Ghosh et al. (2002)) which attempt to capture additional features of the internal dynamics of the rapid stretching process for long flexible chains. As the concentration of dissolved polymer chains is increased, entanglement effects also dramatically modify the extensional rheology of the viscoelastic fluid. However, recent experiments have shown that an exponential period of capillary-induced thinning, followed by finite time

breakup still occurs (Bhattacharjee et al. (2003)). A significant benefit of the present experimental configuration and accompanying analytical description is precisely that the characteristics of the final breakup process sensitively depend on the nonlinear description of the test fluid that is used. Thus analysis of the capillary-thinning and breakup of polymer solutions provides for a promising testing ground to better understand some of the important nonlinear features of viscoelastic constitutive equations at large strains.

We are grateful to the Deutsche Forschungsgemeinschaft, who funded M. F. and J. L.'s visit to Essen through grant SFB237. G.H.M. and C.C. would like to thank the Dupont-MIT Alliance and the NSF-MRI program for supporting the experimental portion of this work. Daniel Bonn contributed a careful reading of the manuscript and very useful discussions. The authors are indebted to John Hinch for helping improve the presentation substantially.

Appendix A. Rheological characterisation of viscoelastic test fluids

The viscoelastic solution used for the capillary break-up experiments in figures 1, 6, and 11 consists of a dilute solution ($c = 0.050 \text{ wt}\%$; $c/c^* = 0.44$) of a polystyrene standard (molar mass $M_w = 2.0 \times 10^6 \text{ g/mol}$, $M_w/M_n = 1.03$, Pressure Chemical) dissolved in oligomeric styrene (Piccolastic A5 Resin, Hercules). This is an example of the class of fluids identified as “Boger fluids”. The polymer was dissolved directly in the oligomeric resin, and the fluid was gently rolled for 2 months to ensure a homogeneous mixture. The shear and extensional rheology of this ideal elastic fluid was also studied in detail in Anna et al. (2001), in which it was identified by the acronym “SM1”. It should be noted that the zero shear rate viscosity and longest relaxation time have increased since the fluid was originally characterised four years ago. This is common in such fluids due

to the slow and irreversible polymerisation of the oligomeric solvent by residual catalyst and/or UV light.

The low viscosity polymer solution in figure 2 was prepared by dissolving 0.01 wt% linear polyacrylamide (Praestol 2540, Stockhausen) with a reported molar mass $M_w = 14.0 \times 10^6 \text{ g/mol}$ in deionised water. Using the reported degree of hydrolysis for this polyacrylamide grade (40%) with a repeat unit mass of 71.4 g/mol and a coil expansion coefficient of $C_\infty = 12.9$ we compute the critical overlap concentration for this fluid to be approximately $c^* = 0.0134 \text{ wt\%}$. The test fluid is thus in the dilute regime with $c/c^* = 0.75$. The fluid was shaken gently for 1 week to ensure a homogeneous mixture.

The rheology of both fluids in both steady and dynamic shear flows was characterised using a TA Instruments AR1000N cone-and-plate rheometer. The longest relaxation time λ and solvent and polymer contributions to the viscosity (η_s and $\eta_p = \eta_0 - \eta_s$) were obtained by fitting the linear viscoelastic moduli $G'(\omega)$ and $G''(\omega)$ to the predictions of the Rouse-Zimm model for dilute solutions:

$$G' = \frac{cN_A k_B T}{M_w} \sum_{i=1}^{N_m} \frac{(\lambda_i \omega)^2}{1 + (\lambda_i \omega)^2} \quad (\text{A } 1)$$

$$G'' = \eta_s \omega + \frac{cN_A k_B T}{M_w} \sum_{i=1}^{N_m} \frac{\lambda_i \omega}{1 + (\lambda_i \omega)^2}. \quad (\text{A } 2)$$

The spectrum of relaxation times, λ_i are related to the longest (Zimm) relaxation time (denoted in the manuscript by λ) by a recursion relationship of the form

$$\lambda_i = \lambda / i^{2+\tilde{\sigma}} \quad \text{for } i = 2, \dots, N_m \quad (\text{A } 3)$$

where $\tilde{\sigma}$ is a measure of the hydrodynamic interaction between the segments of the polymer chain and the surrounding solvent. This parameter is related to the hydrodynamic interaction parameter h^* of the Zimm model by a correlation originally published by Thurston (Bird et al. (1987)). Varying the hydrodynamic interaction parameter in the

range $0 \leq h^* \leq 0.25$ allows better agreement between the experimental and fitted curves at intermediate angular frequencies ω ; for further details see Anna et al. (2001). The zero shear rate viscosity is obtained from eq. (A 2) by taking the limit of G''/ω as $\omega \rightarrow 0$, and the polymer contribution to the viscosity is given by

$$\eta_p = \frac{cN_A k_B T}{M_w} \sum_{i=1}^{N_m} \lambda_i \quad (\text{A } 4)$$

The number of modes, N_m can be varied depending on the resolution of the viscoelastic spectrum of the polymer solution that is desired. The Hookean dumbbell corresponds to $N_m = 1$.

Detailed experiments on polystyrene solutions (Amelar et al. (1991)) shows that the molecular mass associated with a single spring is $5,000 - 10,000 \text{ g/mol}$; suggesting that for the polystyrene used in the present study $N_m \approx 200$. In practise, given the rapid decay of the higher relaxation modes given by eq. (A 3) and the range of frequencies over which the linear viscoelastic moduli can be obtained, we find $9 \leq N_m \leq 15$ is sufficient. Using equations (A 1 - A 4) we determined the model values reported in the captions of figures 1 and 2.

If we now consider the effect of a discrete spectrum on capillary thinning experiments, we find that the local rate of stretching in the cylindrical thread arising from the elastocapillary balance is sufficiently weak (in dimensional form $\dot{\epsilon} = 2/(3\lambda)$), that all higher modal contributions to the stress (of the form of eqs. 2.3, 2.4) decay away rapidly. They do not contribute significantly to the total elastic stress because the convective derivative terms that signify stretching for the higher modes are of the form $(2De)v'/i^{2+\bar{\sigma}}$, which all decay rapidly for $i > 1$

The capillary break-up experiments were carried out using a CaBER-1 extensional rheometer (Cambridge Polymer Group). The images presented in figures 1 and 11 were recorded with a CCD-videocamera (Pulnix TM1) and a digital video recorder. For the

digitised close-up in figure 11, the camera was equipped with a long-working distance microscope extension (K2, Infinity Optical). All experiments were conducted at $T = 25^\circ\text{C}$.

REFERENCES

- Amarouchene, Y., Bonn, D., Meunier, J. & Kellay, H. 2001 Inhibition of the finite-time singularity during droplet fission of a polymeric fluid. *Phys. Rev. Lett.* **86**, 3558-3561.
- Amelar, S., Eastman, C., Lodge, T., & Vonmeerwall, E. 1991 How Good Is The Bead-Spring Model? *J. Non-Cryst. Solids*, **131** (Part 2), 551-555.
- Anna, S.L. & McKinley, G.H. 2001 Elasto-capillary thinning and breakup of model elastic liquids. *J. Rheol.* **45**, 115-138.
- Anna, S.L., McKinley, G.H., Nguyen, D.A., Sridhar, T., Muller, S.J., Huang, J. & James, D.F. 2001 An Inter-Laboratory Comparison of Measurements from Filament-Stretching Rheometers Using Common Test Fluids. *J. Rheol.* **45**, 83-114.
- Bazilevskii, A.V., Entov, V.M., Lerner, M.M. & Rozhkov, A.N. 1997 Failure of polymer solution filaments. *Polym. Sci. Ser. A* **39**, 316-324.
- Bazilevsky, A.V., Entov, V.M., & Rozhkov, A.N. 1990 Liquid Filament Microrheometer and Some of its Applications. Third European Rheology Conference, D. R. Oliver (ed.), Elsevier Applied Science, 41-43.
- Bazilevskii, A.V., Voronkov, S.I., Entov, V.M. & Rozhkov, A.N. 1981 Orientational effects in the decomposition of streams and strands of diluted polymer solutions. *Sov. Phys. Dokl.* **26**, 333-335.
- Bhattacharjee, P.K., Nguyen, D.A., McKinley, G.H. & Sridhar, T. 2003 Extensional Stress Growth and Stress Relaxation in Entangled Polymer Solutions. *J. Rheol.* **47**, 269-290.
- Bird, R.B., Armstrong, R.C. & Hassager O. 1987 *Dynamics of polymeric liquids, Vol. 1: Fluid Mechanics, Vol. 2: Kinetic Theory*. Wiley, New York.
- Bousfield, D.W., Keunings, R., Marrucci, G. & Denn, M.M. 1986 Nonlinear analysis of the surface tension driven breakup of viscoelastic filaments. *J. Non-Newtonian Fluid Mech.* **21**, 79-97.

- Chang, H.C., Demekhin, E.A. & E. Kalaidin, E. 1999 Iterated stretching of viscoelastic jets. *Phys. Fluids* **11**, 1717-1737.
- Christanti, Y.M. & Walker, L. 2001 Surface tension driven jet break up of strain-hardening polymer solutions. *J. Non-Newtonian Fluid Mech.* **100**, 9-26.
- Christanti, Y.M. & Walker, L. 2002 Effect of Fluid Relaxation Time on Jet Breakup due to a Forced Disturbance of Polymer Solutions. *J. Rheol.* **46**, 733-748.
- Cooper-White, J.J., Fagan, J.E., Tirtaatmadja, V., Lester, D.R., & Boger, D.V. 2002 Drop Formation Dynamics of Constant Low Viscosity Elastic Fluids. *J. Non-Newtonian Fluid Mech.* **106**, 29-59.
- Eggers, J. 1997 Nonlinear dynamics and breakup of free surface flows. *Rev. Mod. Phys.* **69**, 865-929.
- Eggers, J. & Dupont, T.F. 1994 Drop formation in a one-dimensional model of the Navier-Stokes equation. *J. Fluid Mech.* **262**, 205-221.
- Eggers, J., Fontelos, M. & Li, J. 2005 Pinching of the three-dimensional, axisymmetric Oldroyd B equation. *Unpublished*.
- Entov, V.M. & Hinch, E.J. 1997 Effect of a spectrum of relaxation times on the capillary thinning of a filament of elastic liquid. *J. Non-Newtonian Fluid Mech.* **72**, 31-53.
- Entov, V.M. & Yarin, A.L. 1984 Influence of Elastic Stresses on the Capillary Breakup of Dilute Polymer Solutions. *Fluid Dyn.* **19**, 21-29, transl. from *Izvestiya Akademii Nauk SSSR, Mekhanika Zhidkosti Gaza* **19**, 27-35.
- Fontelos, M. 2003 Break-up and no break-up in a family of models for the evolution of viscoelastic jets. *ZAMP* **54**, 84-111.
- Fontelos, M.A. & Li, J. 2004, On the evolution and rupture of filaments in Giesekus and FENE models, *J. non-Newtonian Fluid Mech.* **118**, 1-16.
- Forest, M. G. & Wang, Q. 1990 Change-of-type behavior in viscoelastic slender jet models. *J. Theor. Comp. Fluid Dyn.* **2**, 1-25.
- Goldin, M., Yerushalmi, J., Pfeffer, R. & Shinnar, R. 1969 Breakup of a laminar capillary jet of a viscoelastic fluid. *J. Fluid Mech.* **38**, 689-711.

- Goren, S.L. & Gottlieb, M. 1982 Surface-tension-driven breakup of viscoelastic liquid threads. *J. Fluid Mech.* **120**, 245-266.
- Ghosh, I., Joo, Y.L., McKinley, G.H., Brown, R.A. & Armstrong, R.C. 2002 A New Model for Dilute Polymer Solutions in Flows with Strong Extensional Components. *J. Rheol.* **45**, 1057-1089.
- Harlen, O.G., 1996 Numerical Simulation of the Filament Stretching Rheometer, Presentation at the Isaac Newton Institute program on *Dynamics of Complex Fluids*, Cambridge UK.
- Kolte, M.I. & Szabo, P. 1999 Capillary Thinning of Polymeric Filaments, *J. Rheol.* **43**, 609-626.
- Kopito, L.E. & Kosasky, H.J. 1979 The Tackiness Rheometer determination of the Viscoelasticity of Cervical Mucus. Human Ovulation, E. S. F. Hafez (ed.), Elsevier/North-Holland, Amsterdam, 351-361.
- Larson, R.G. 1992 Instabilities in viscoelastic flows. *Rheologica Acta* **31**, 213-263.
- Lhuillier, D. 2001 A possible alternative to the FENE dumbbell model of dilute polymer solutions. *J. Non-Newtonian Fluid Mech.* **97**, 87-96.
- Li, J. & Fontelos, M. 2003 Drop dynamics on the beads-on-string structure for viscoelastic jets: A numerical study. *Phys. Fluids* **15**, 922-937.
- Li, L., Larson, R.G. & Sridhar, T. 2000 Brownian Dynamics Simulations of Dilute Polystyrene Solutions. *J. Rheol.* **44**, 291-323.
- Renardy, M. 1994 Some comments on the surface-tension driven break-up (or the lack of it) of viscoelastic jets. *J. Non-Newtonian Fluid Mech.* **51**, 97-101.
- Renardy, M. 1995 A numerical study of the asymptotic evolution and breakup of Newtonian and viscoelastic jets. *J. Non-Newtonian Fluid Mech.* **59**, 267-282.
- Renardy, M. 2001 Self-similar breakup of a Giesekus jet. *J. Non-Newtonian Fluid Mech.* **97**, 283-293.
- Renardy, M. 2002 Similarity Solutions For Jet Breakup for Various Models of Viscoelastic Fluids. *J. Non-Newtonian Fluid Mech.* **104**, 65-74.
- Shaqfeh, E.S.G., McKinley, G.H., Woo, N., Nguyen, D.A. & Sridhar, T. 2004 On the Polymer Entropic Force Singularity and its Relationship to Extensional Stress Relaxation and Elastic Recoil. *J. Rheol.* **48** 209-221.

- Shipman, R.W.G., Denn, M.M. & Keunings, R. J. 1991 Mechanics of the falling plate extensional rheometer. *J. Non-Newtonian Fluid Mech.*, **40**, 281-288.
- Spiegelberg, S.H., Ables, D.C. & McKinley, G.H. 1996 The role of end-effects on measurements of extensional viscosity in viscoelastic polymer solutions with a filament stretching rheometer. *J. Non-Newtonian Fluid Mech.* **64**, 229-267.
- Stelter, M., Brenn, G., Yarin, A. L., Singh, R. P., & Durst, F. 2000 Validation and Application of a Novel Elongational Device for Polymer Solutions. *J. Rheol.* **44**, 595-616.
- Stokes, Y.M., Tuck, E.O. & Schwartz, L.W. 2000 Extensional fall of a very viscous fluid drop. *Q. J. Mech. Appl. Math.* **53**, 565-582.
- Tripathi, A., Whittingstall, P. & McKinley, G. H. 2000 Using Filament Stretching Rheometry to Predict Strand Formation and "Processability" in Adhesives and Other Non-Newtonian Fluids. *Rheologica Acta* **39**, 321-337.
- von Ohnesorge, W. 1936 Die Bildung von Tropfen an Düsen und die Auflösung flüssiger Strahlen. *ZAMM* **16**, 355-358.
- Yao, M. & McKinley, G.H. 1998 Numerical Simulation of Extensional Deformations of Viscoelastic Liquid Bridges in Filament Stretching Devices. *J. Non-Newtonian Fluid Mech.* **74**(1-3), 47-88.
- Yarin, A.L. 1993 *Free liquid jets and films: hydrodynamics and rheology*. Wiley, New York.